HEP'99 # 6_141
Submitted to Pa 6, 7
Pl 6, 7

DELPHI 99-77 CONF 264
15 June 1999

Photon Events with Missing Energy at LEP 2

Preliminary

DELPHI Collaboration

Paper submitted to the HEP'99 Conference
Tampere, Finland, July 15-21

Photon Events with Missing Energy at LEP2.

The DELPHI Collaboration

P. Checchia [4], **A. De Min** [5], **E. Falk** [2], **P. Ferrari** [1], **V. Hedberg** [5], **S. Katsanevas** [6], **M. Margoni** [4], **C. Matteuzzi** [1], **F. Mazzucato** [4], **A. Perrotta** [3].

Abstract

A study has been made of the production of single photons in the reaction $e^+e^- \to \gamma \ + \ \textit{invisible particles}$ at $\sqrt{s} = 183$ GeV and 189 GeV and a previous analysis of events with a single non-pointing photon or with multi-photon final states accompanied by missing energy has been updated with 189 GeV data. The data was collected with the DELPHI detector and corresponds to an integrated luminosity of about 51 pb^{-1} and 158 pb^{-1} at the two energies. The number of light neutrino families is measured. The absence of an excess of events beyond that expected from Standard Model processes is used to set limits on new physics as described by supersymmetric and composite models. A limit on the gravitational scale is also determined.

[1] Università e Sezione INFN, Milano, Italy.

[2] Lund University, Lund, Sweden.

[3] Università e Sezione INFN, Bologna, Italy.

[4] Università e Sezione INFN, Padova, Italy.

[5] CERN, Geneva, Switzerland.

[6] Université Claude Bernard de Lyon IPNL, Lyon, France.

1 Introduction

At LEP2, the Standard Model predicts that events with one or more photons and invisible particles are produced exclusively by the reaction $e^+e^- \to \nu\bar{\nu}\gamma(\gamma)$ which receives a contribution from Z-exchange in the s-channel with single- or multi-photon emission from the initial state electrons and from the t-channel W exchange, with the photon(s) radiated from the beam electrons or the exchanged W.

Beyond the Standard Model, contributions to the γ + *missing energy* final state could come from a new generation of neutrinos, from the radiative production of some other neutral weakly interacting particle or from a new particle decaying into a photon. Theories of supersymmetry (SUSY) predict the existence of particles, such as the neutralino, which would give origin to a final state with missing energy and a photon if the lightest neutralino decays into $\tilde{G}\gamma$ with an essentially massless gravitino ($m_{\tilde{G}} < 1$ eV/c^2). Several results have been published on this topic [1][2][3]. If the gravitino is the lightest SUSY particle and all other supersymmetric particles are too heavy to be produced, the expected cross-section for $e^+e^- \to \tilde{G}\tilde{G}\gamma$ can be used to set a lower limit on the gravitino mass [4]. In the same theoretical framework multi-photon final states with missing energy would be a signature for neutralino pair-production, i.e. reaction of type $\mathrm{e^+e^-} \to \tilde{\chi}_1^0\tilde{\chi}_1^0 \to \tilde{G}\tilde{G}\gamma\gamma$ and $\mathrm{e^+e^-} \to \tilde{\chi}_2^0\tilde{\chi}_2^0 \to \tilde{\chi}_1^0\tilde{\chi}_1^0\gamma\gamma$. In case of long neutralino lifetimes the photons would not be originated at the beam interaction region and would present large impact parameter. For mean decay paths larger than the detector scale a single non-pointing photon is expected.

In the study presented here, the single- and the multi-photon final states at LEP2 are used to explore the existence of possible new particles. After a brief description of the detectors used in the analysis and the selection criteria, a measurement of the number of neutrino families is made and limits on non-Standard Model physics, such as compositeness [5], high-dimensional gravitons [6][7][8] and supersymmetric particles [9], are presented.

The analysis described in this paper concerns single-photon events collected at $\sqrt{s} = 183$ GeV and $\sqrt{s} = 189$ GeV, with integrated luminosities of 51 pb^{-1} and 158 pb^{-1}, respectively. Single non-pointing photons and multi-photon events have also been studied, but in this case the analysis is restricted to the data taken at $\sqrt{s} = 189$ GeV, since the results obtained at lower energies have already been published elsewhere [10]. The limits set on new phenomena also take into account the lower energy data.

2 The DELPHI detector

The general criteria for the selection of events are based mainly on the electromagnetic calorimeters and the tracking system of the DELPHI experiment [11]. All three major electromagnetic calorimeters in DELPHI, the High density Projection Chamber (HPC), the Forward ElectroMagnetic Calorimeter (FEMC) and the Small angle TIle Calorimeter (STIC), have been used in the single-photon reconstruction. The barrel region is covered by the HPC, which is a gas sampling calorimeter which samples a shower nine times longitudinally. FEMC is made up of an array of 4532 lead glass blocks in each endcap. The energy resolution of the calorimeter is degraded by the material in front of it, which causes photon conversions and even preshowers. The very forward luminosity monitor STIC [12] consists of two cylindrical lead-scintillator calorimeters read out by wavelength-

shifting fibers. Two layers of scintillators mounted on the front of each STIC calorimeter together with a smaller ringshaped scintillator mounted directly on the beampipe, provide $e-\gamma$ separation. The angular coverage of these calorimeters and the energy resolution are given in Table 1 and the detailed characteristics and performances are described in [11].

Three different triggers are used in DELPHI to select single-photon events. The HPC trigger for purely neutral final states uses a plane of scintillators inserted into one of the HPC sampling gaps at a depth of around 4.5 X_0. A second level trigger decision is produced from the signals of analog electronics and is based on a coincidence pattern inside the HPC module. The trigger efficiency has been measured with Compton and Bhabha events. It is strongly dependent on the photon energy up to ∼12 GeV, with about 30% efficiency at 4 GeV and above 80% when $E_\gamma > 30$ GeV. It reaches a maximum of 87% at $E_\gamma \simeq E_{\rm beam}$. This efficiency does not include losses due to the cracks between modules of the HPC detector. The FEMC trigger requires an energy deposition of at least 2.5 GeV. The efficiency increases with energy and is ∼97% at 18 GeV. Correlated noise in several adjacent channels causes fake triggers, but these can be rejected offline with high efficiency by algorithms that take into account the lead glass shower pattern. The STIC trigger requires an energy deposition of at least 15 GeV and reaches maximum efficiency at 30 GeV. The trigger efficiency has been measured with samples of photons from $e^+e^-\gamma$ and $q\bar{q}\gamma$ events. The efficiency varies between 74% and 27% in the angular region used in the analysis.

In addition to the electromagnetic calorimeters, the DELPHI tracking system, was used to reject events in which charged particles are produced. The main tracking devices are the Time Projection Chamber (TPC) and the microVertex silicon Detector (VD) and its extension into the forward region, the so-called Very Forward Tracker (VFT). The two latter detectors are also used for electron/photon separation by vetoing photon candidates which can be associated with hits in these detectors.

Finally, the hadron calorimeter (HCAL) and its Cathode-Read-Out (CRO) system were used to reject cosmics and to provide photon/hadron separation, while the DELPHI Hermeticity Taggers were used to ensure complete detector hermeticity for additional neutral particles.

	Type	Angular coverage	σ_E/E	χ_0
STIC:	Lead/scint.	$2^\circ < \theta < 10^\circ$, $170^\circ < \theta < 178^\circ$	$0.0152 \oplus (0.135/\sqrt{E})$	27
FEMC:	Leadglass	$10^\circ < \theta < 37^\circ$, $143^\circ < \theta < 170^\circ$	$0.03 \oplus (0.12/\sqrt{E}) \oplus (0.11/E)$	20
HPC:	Lead/gas	$40^\circ < \theta < 140^\circ$	$0.043 \oplus (0.32/\sqrt{E})$	18

Table 1: Polar angle coverage, energy resolution (where E is in GeV) and thickness (in radiation lenghts) of the electromagnetic calorimeters in DELPHI.

3 Event selection

3.1 Single-photon events

The basic selection criteria of events are the same for the three electromagnetic calorimeters: no charged tracks detected and no electromagnetic showers apart from the shower from the single-photon candidate. However, the details of the selection vary somewhat for the different electromagnetic calorimeters:

- Events with a photon in the HPC were selected by requiring a shower having an energy above 6 GeV and a polar angle in the interval $45^\circ < \theta < 135^\circ$ and no charged tracks. The shower were required to satisfy some conditions meant to define good electromagnetic shape [2]. Background from radiative Bhabha events and Compton events were rejected by requiring that any second electromagnetic shower in the event was in the HPC and that it was within 20° of the first one. Cosmic rays were rejected by the charged track requirement and by the hadron calorimeter. The event was rejected if there were two or more hadronic showers. If only one HCAL shower was present, the event was retained if the shower was consistent with being caused by punch-through of the electromagnetic shower. A constraint on the γ direction was imposed, requiring that the line of flight and the shower direction measured in the calorimeter coincided within 15°.
  The photon identification efficiency depends on the criteria applied to require a good electromagnetic shower. It was determined on the basis of a Monte Carlo sample of events passed through the complete simulation of the DELPHI detector [13]. The efficiency depends on the photon energy and it ranges from $\sim$45% at low E_γ to $\sim$78% for $E_\gamma > 15$ GeV.

- Events with at least one shower in FEMC with an energy above 18 GeV and a polar angle in the intervals $12^\circ < \theta < 32^\circ$ or $148^\circ < \theta < 168^\circ$ were also selected. Showers in the lower and upper parts of FEMC were discarded because of the large amount of material in front of FEMC due to the STIC and the TPC detectors. In order to separate electrons from photons, the FEMC shower was extrapolated to the interaction point and the event was rejected if hits in the silicon microvertex detectors (VD and VFT) could be associated with the shower.
  The material in front of FEMC meant that about half of the photons preshowered before reaching the calorimeter. Most of the preshower was contained in a cone of about 15° around the largest shower and the selection took this into account by requiring no charged tracks, no other electromagnetic showers and no hadronic showers outside a 15° cone. If there were no charged tracks inside the cone either, i.e., the photon had not preshowered, it was required that only one FEMC shower was present in the event. If, on the other hand, charged tracks were present in the cone, more than one FEMC shower were allowed and their momentum vectors were added to that of the largest shower.
  The requirement of no electromagnetic showers outside the cone greatly reduced the background of radiative Bhabha and Compton events by rejecting events that had one or both electrons in the acceptance of the experiment. Events due to cosmic rays were rejected by the requirement of no hadronic showers outside the cone. Inside the cone, hadronic energy was allowed only in the first layer of the HCAL.

Most reconstruction and event selection efficiencies in the analysis were taken into account by using Monte Carlo samples passed through the extensive detector simulation package of DELPHI [13]. Some efficiencies, however, were determined from data. In particular, the requirements of no electromagnetic or hadronic showers and no charged tracks were studied. A sample of events triggered at random and a sample of back-to-back Bhabha events with the electrons in STIC were used for this purpose. It was found that noise and machine background caused showers and tracks which would veto about 14% of the good single-photon events.

- Single photons in STIC were selected by requiring one shower with an energy of at least 27 GeV in one of the two STIC calorimeters and with $3.8^\circ < \theta < 8^\circ$ or $172^\circ < \theta < 176.2^\circ$ and no other electromagnetic showers, no hadronic showers and no charged tracks in the event. It was furthermore required that all single-photon candidates had satisfied the STIC single-photon trigger and that there was no signal in at least one of the two scintillator planes in front of the shower. A requirement of no signal in the small scintillators mounted on the beampipe made it possible to reject some of the radiative $ee\gamma$ background. In spite of the scintillator requirements, the huge background of off-energy electrons made it necessary to introduce an energy-dependent θ-cut in such away that $\theta > 9.2^\circ - 9^\circ x_\gamma$ for $x_\gamma < 0.6$ where $x_\gamma = E_\gamma / E_{beam}$, i.e., the photon energy in units of the incident beam energy. The trigger efficiency in the STIC acceptance was discussed in Section 2. The offline photon identification and reconstruction resulted in an additional loss of 5% of the photons. The selection of events with no shower in STIC and no tracks introduced similar losses as those in the FEMC analysis and were estimated with the same methods.

3.2 Non-pointing single-photon events

The fine granularity of the HPC calorimeter provides a precise reconstruction of the axis direction in electromagnetic showers. This feature was used to select events with a single photon whose flight direction does not point to the beam interaction region. Events with a single non-pointing photon are expected when two neutral particles are produced which subsequently decay into a photon and a invisible particle with large mean decay paths (> 4 m).

Events of this kind are searched for by requiring one photon in the HPC calorimeter with $E_\gamma > 10$ GeV and impact parameter exceeding 40 cm. Cosmic events, which represent the main experimental background, are largely reduced by vetoing on isolated hits or tracks in the Hermeticity Taggers and in the Hadron Calorimeter Cathode-Read-Out. More details on the precise event selection can be found in [10], were the analysis of the data samples collected at centre-of-mass energies up to $\sqrt{s} = 183$ GeV is described. The same analysis has been applied to the data sample taken at $\sqrt{s} = 189$ GeV.

3.3 Multi-photon events

A study of final states with at least two photons and missing energy at $\sqrt{s} = 189$ GeV has also been made.

As for non-pointing single photons, the physics motivations and the selection criteria have been discussed in detail in the published paper [10] dedicated to the analysis of the data taken at centre-of-mass energies up to 183 GeV. Here only a brief update of the results is given on the basis of the 1998 data, while the data analysis has been kept unchanged.

As in [10], the selection of multi-photon final states is based on a two-step procedure.

- In a first step all events having at least two photons with $x_\gamma > 0.05$ and missing transverse energy were preselected. Very loose cuts on the photons polar angle and acoplanarity were adopted for the selection of this sample, which was used to monitor the modeling of the $e^+e^- \to \nu\nu\gamma\gamma(\gamma)$ process by the Koralz 4.02 generator.

- In a second step these criteria were tightened in order to improve the experimental sensitivity for possible signals of supersymmetry, such as the $e^+e^- \to \tilde{\chi}^0_1\tilde{\chi}^0_1 \to \tilde{G}\tilde{G}\gamma\gamma$ or $e^+e^- \to \tilde{\chi}^0_2\tilde{\chi}^0_2 \to \tilde{\chi}^0_1\tilde{\chi}^0_1\gamma\gamma$ processes. This was achieved by imposing more stringent requirements on the photon polar angles as well as on the event missing mass and transverse momentum.

More details on the event selection can be found in [10].

4 Real and simulated data samples

Apart from the $e^+e^- \to \nu\bar{\nu}\gamma(\gamma)$ process, single-photon events can be faked by the QED reaction $e^+e^- \to e^+e^-\gamma$ where the two electrons escape undetected along the beampipe or the electrons are lost by not being detected by the experiment.

This process has a very high cross-section, decreasing rapidly when the energy (E_γ) and the polar angle (θ_γ) of the photon increases. The behaviour of this QED background together with the rapidly varying efficiencies at low energies are the reasons why different energy cuts had to be applied for photons in the three calorimeters. In the final analysis it was required that $x_\gamma > 0.06$ (HPC), $x_\gamma > 0.2$ (FEMC) and $x_\gamma > 0.3$ (STIC).

The critical parameter in the rejection of the $e^+e^-\gamma$ background is the polar angle at which the electrons start being seen in the STIC detector. This detector reconstructs electrons down to $\theta = 38$ mrad and in addition the scintillator counters mounted on the beampipe can be used to reject events with electrons down to 31 mrad. Simulations have shown that even at lower angles (down to 17 mrad) a large fraction of the electrons are detectable because they interact with a tungsten shield mounted inside the beampipe and leak enough energy into the STIC to make it possible to reject the events.

The remaining background from the $e^+e^-\gamma$ process in the acceptance of the STIC and FEMC detectors was calculated with a Monte Carlo program [14] and two different event topologies were observed. Either both electrons were below the STIC acceptance or one of the electrons was in the DELPHI acceptance where it was wrongly identified as a photon, and the photon was lost in the cracks between the electromagnetic calorimeters. The first topology gives background at low photon energy while the second one produces fake photon events at high energy. In the HPC acceptance an analytical calculation [15] showed that the $e^+e^-\gamma$ background was negligible.

In STIC, an additional background is the single electrons produced by interactions between the beam particles and residual gas molecules in the LEP beampipe. In these

$e \to e\gamma$ events the photons are always lost in the beampipe while the off-energy electrons are bent into the STIC acceptance by the low-beta quadrupoles close to DELPHI. The rate of this background is so large that it was not possible to provide a $\gamma - e$ separation powerful enough to eliminate completely this background. A simulation has been made of off-energy electron production [16] but it could not be used in the analysis since the vacuum pressure around the LEP ring was not known to the required precision. Instead a background sample was collected with a trigger similar to the photon trigger but without the requirement of an absence of signal in the scintillators and from this sample the remaining off-energy electron background was estimated.

The contribution from other processes such as $\gamma\gamma$ collisions, $e^+e^- \to \gamma\gamma\gamma$, cosmic ray events, $e^+e^- \to \mu^+\mu^-\gamma$ and $e^+e^- \to \tau^+\tau^-\gamma$ has also been calculated.

The $\nu\bar{\nu}\gamma(\gamma)$ process was simulated by the KORALZ [17] and NUNUGPV [18] programs.

A detailed discussion on the backgrounds for the non-pointing single-photon events and for the multi-photon events is contained in [10].

	HPC		FEMC		STIC	
θ_γ:	$45° - 135°$		$12° - 32°$, $148° - 168°$		$3.8° - 8.0°$, $172° - 176.2°$	
x_γ:	> 0.06		0.2 - 0.9		0.3 - 0.9	
$\sqrt{s}$:	182.7 GeV	188.7 GeV	182.7 GeV	188.7 GeV	182.7 GeV	188.7 GeV
Luminosity:	50.2 pb^{-1}	154.7 pb^{-1}	49.2 pb^{-1}	157.7 pb^{-1}	51.4 pb^{-1}	157.3 pb^{-1}
$N_{observed}$:	54	145	65	155	32	94
$N_{background}$:	0	0	3.5	3.7	3.6	6.5
$N_{e^+e^-\to\nu\bar{\nu}\gamma}$:	59.5	157.7	55.0	153.4	32.4	95.3
σ_{meas} (pb)	1.85±0.25	1.80±0.15	2.33±0.31	1.92±0.16	1.27±0.25	1.41±0.15
$\sigma_{\nu\bar{\nu}\gamma}$ (pb)	2.04	1.97	2.08	1.94	1.50	1.42
N_ν	2.70±0.40	2.74±0.23	3.36±0.44	2.97±0.25	2.54±0.51	2.98±0.32

Table 2: Number of selected and expected events, measured and calculated cross-section for $e^+e^- \to \nu\bar{\nu}\gamma(\gamma)$ (for three neutrino generations) and the number of neutrino generations calculated from the cross-sections. The errors are statistical only.

5 Comparison with the Standard Model expectations

5.1 Single-photon cross-section

The final number of expected and observed single-photon events are given in Table 2 and the energy spectrum of the selected events at 189 GeV is shown in Figure 1 together with the expected background and the $\nu\bar{\nu}\gamma$ contribution. In total, 545 single-photon events were observed at 189 GeV and 183 GeV in the three calorimeters, with 571 events expected from known sources. Where relevant for the analysis, the samples in the HPC consisting

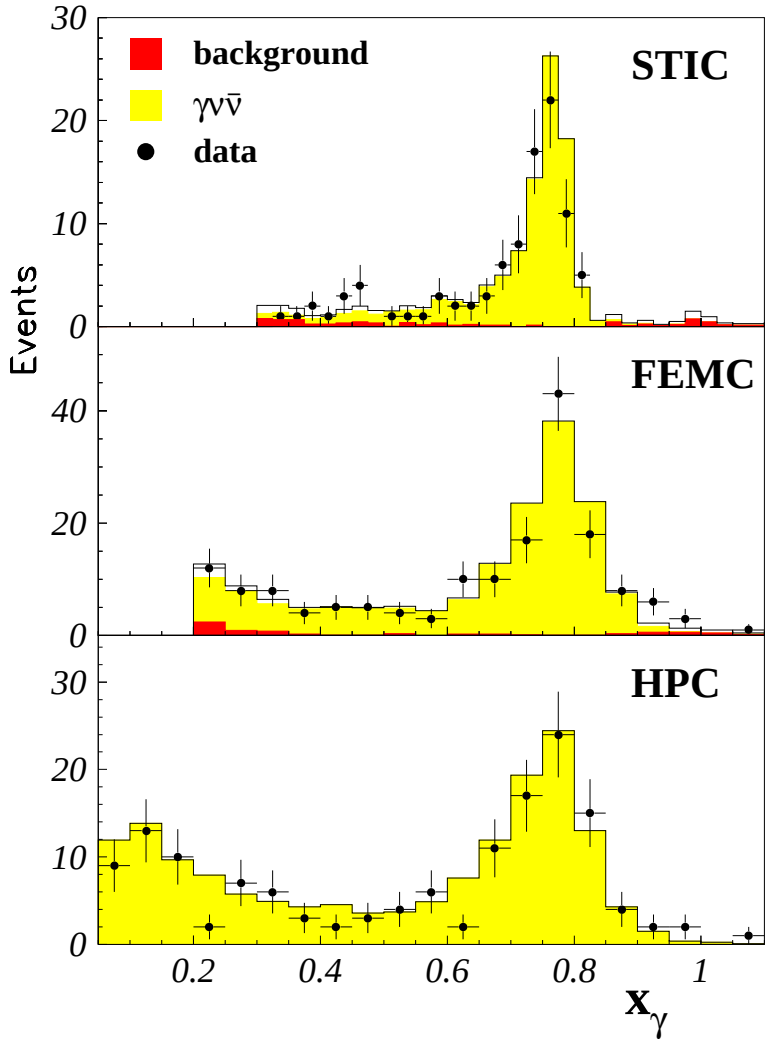

Figure 1: x_γ of selected single photons at 189 GeV in the three calorimeters STIC, FEMC and HPC. The light shaded area is the expected spectrum from $e^+e^- \to \nu\bar{\nu}\gamma$ and the dark shaded area is the total background from other sources.

of 10 events at 161 GeV and 11 events at 172 GeV were also considered (the total collected luminosity was 19.9 pb^{-1}). At these lower energies the number of expected events from Standard Model sources was 15.1 and 10.8 at the two energies respectively [19].

The measured cross-sections for single-photon events after correcting for background and efficiencies are given in Table 2. Events with more than one photon can survive the single-photon selection if the other photons are at low angle ($\theta_\gamma < 38$ mrad), low energy ($E_\gamma < 0.8$ GeV) or within 3, 15 and 20 degrees with respect to the highest energy photon in STIC, FEMC and HPC respectively. The previously mentioned Monte Carlo programs were used to calculate the expected values of the cross-section of the process $e^+e^- \to \nu\bar{\nu}\gamma(\gamma)$ inside the acceptance of each of the three detectors used in the analysis. Figure 2 shows the expected behaviour of the cross-section, calculated with $NUNUGPV$, compared with the values measured with the HPC detector at different LEP energies. The contribution from various sources to the systematic error in the cross-section measurement is given in Table 3. The dominant uncertainty comes from the estimation of trigger and detection efficiencies.

	HPC		FEMC		STIC	
Source	Variation	$\Delta\sigma$	Variation	$\Delta\sigma$	Variation	$\Delta\sigma$
Luminosity	$\pm1\%$	$\pm1\%$	$\pm1\%$	$\pm1\%$	$\pm1\%$	$\pm1\%$
Trigger efficiency	$\pm5\%$	$\pm5\%$	$\pm2\%$	$\pm2\%$	$\pm6\%$	$\pm6\%$
Identification efficiency	$\pm5\%$	$\pm5\%$	$\pm6\%$	$\pm6\%$	$\pm6\%$	$\pm6\%$
Calorimeter energy scale	$\pm5\%$	$\pm4\%$	$\pm5\%$	$\pm5\%$	$\pm0.5\%$	$\pm1\%$
Background	$+25\%$	$+1\%$	$\pm50\%$	$\pm2\%$	$\pm75\%$	$\pm6\%$
Total		$\pm8\%$		$\pm8\%$		$\pm10\%$

Table 3: Contributions to systematic error. The total systematic error is the quadratic sum of the individual errors.

A measurement of the cross-section of the process $e^+e^- \to \nu\bar{\nu}\gamma$ determines the number of light neutrino generations N_ν. DELPHI has previously reported a value of $N_\nu = 2.89 \pm 0.32$ from LEP1 data only [20]. The number of neutrino generations deduced from the LEP2 cross-section measurements are given in Table 2. Averaging the three independent measurements done with the three different calorimeters at 183 GeV and 189 GeV, the number of light neutrino generations becomes:

$$N_\nu = 2.88 \pm 0.13(stat) \pm 0.14(syst)$$

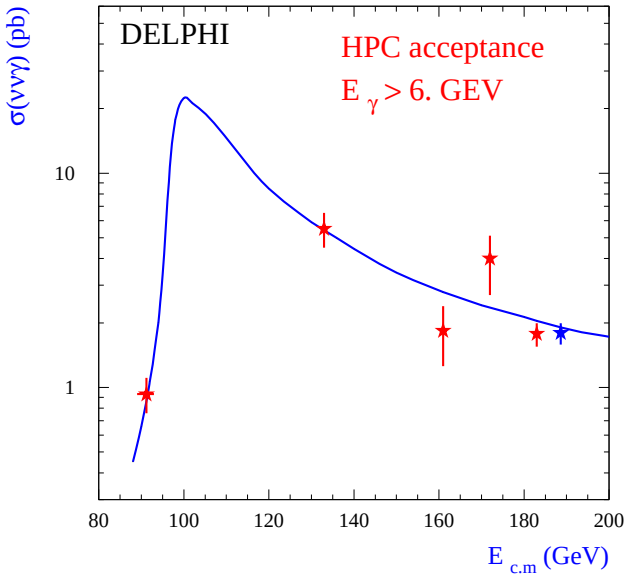

Figure 2: The measured cross-sections at different $\sqrt{s}$ compared to the expected $\sigma(\nu\bar{\nu}\gamma)$ (for three neutrino generations).

5.2 Non-pointing single-photon events and multi-photon events

The number of events with a single non-pointing photon or with multi-photon final states found in the data sample at 189 GeV is compared to the background estimates in Table 4.

The missing mass spectra for the preselected multi-photon events and the expected contribution from $e^+e^- \to \nu\overline{\nu}\gamma\gamma(\gamma)$ as simulated with Koralz are shown in Figure 3. The measured missing mass distribution is in good agreement with the background simulation.

No excess over Standard Model expectations was found in any of the data samples collected at $\sqrt{s} = 189$ GeV. As a consequence these data were combined with lower energy data to extract limits on new physics.

	189 GeV		130-189 GeV	
	Observed	Expected	Observed	Expected
Preselected multi-photon events	17	15.1	27	25.3
$e^+e^- \to \tilde{\chi}^0_1\tilde{\chi}^0_1 \to \tilde{G}\gamma\tilde{G}\gamma$ selection	5	4.4	7	7.1
$e^+e^- \to \tilde{\chi}^0_2\tilde{\chi}^0_2 \to \tilde{\chi}^0_1\gamma\tilde{\chi}^0_1\gamma$ selection	8	5.2	12	8.6
Non-pointing single-photon events	4	5.2	6	7.9

Table 4: The number of observed and expected events from standard model sources in four selected data samples.

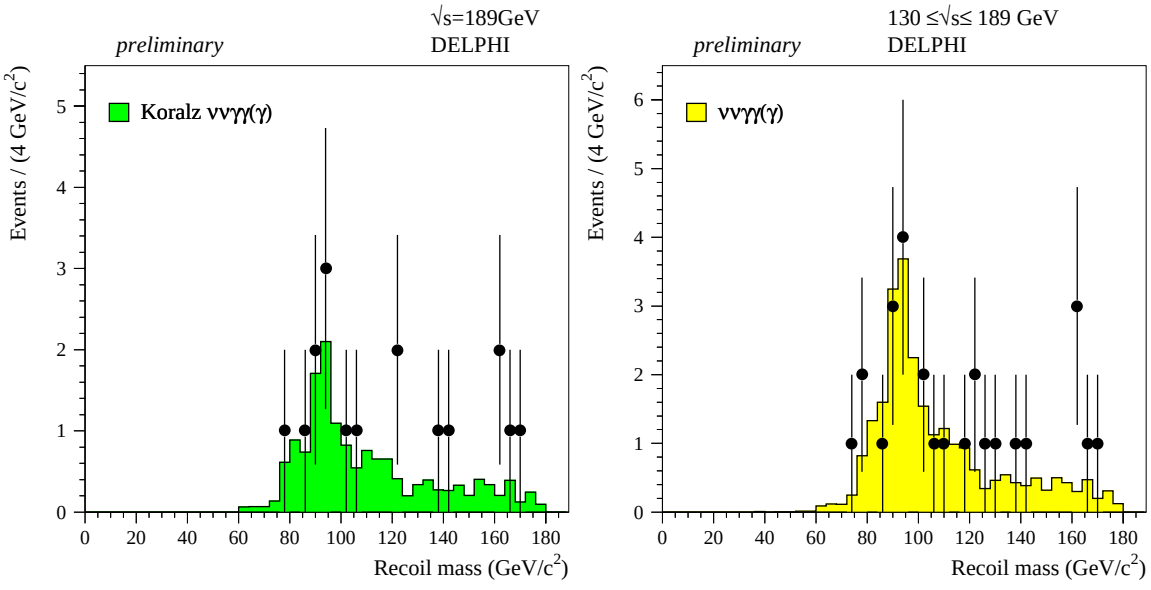

Figure 3: Missing mass distribution observed after multi-photon preselection in the 189 GeV sample (left) and the combined 130-189 GeV sample (right).

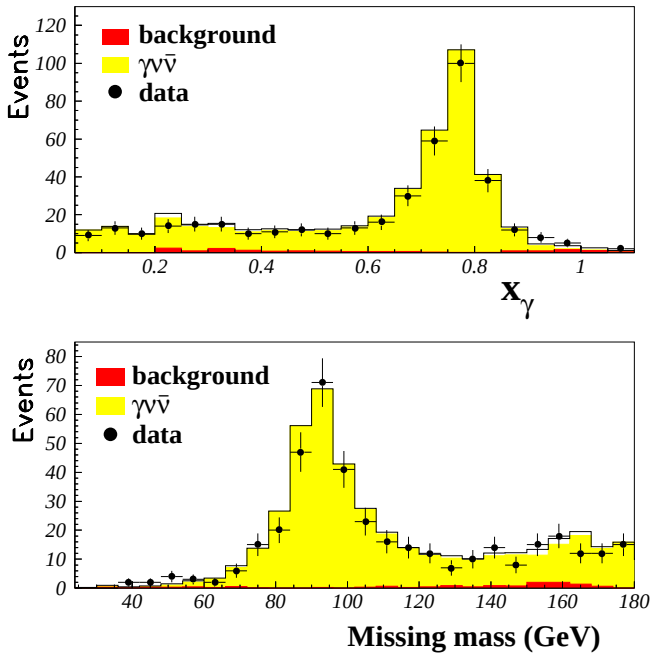

Figure 4: The distributions of x_γ and the recoiling mass against the detected photon for the events at 189 GeV in all three calorimeters.

6 Limits on new phenomena

6.1 Limits on the production of an unknown neutral state

In many previous analyses [2] [20] [21] one has used the observed single-photon candidates to set a limit on the probability of the existence of a new particle, X, produced in association with a photon and being stable or decaying into invisible particles. The limit is calculated from the recoil mass distribution (Figure 4) of the 394 single γ at 189 GeV in the angular region $3.8° < \theta < 176.2°$ and taking into account the expected contributions from the Standard Model. The limit is valid when the intrinsic width of the X particle is negligible compared to the detector resolution (the recoil mass resolution varies between 10 GeV at the Z^0 peak to 1 GeV at high masses). The upper limit at the 95% confidence level of the cross-section for $e^+e^- \rightarrow \gamma$+X is given in Figure 5 for photons in the HPC region and in all three calorimeters combined. In the latter case an assumption of an ISR-like photon angular distribution has been made to correct for the regions between the calorimeters.

6.2 Limits on compositeness

Composite models predict several new particles which do not exist in the Standard Model. A specific Preon Model is considered in this analysis [5]. This model considers leptons, quarks and weak bosons as composite particles. Some of the predicted new particles contribute to the cross-section of the process $e^+e^- \rightarrow \gamma + inv$. At a relatively light mass scale, it predicts the existence of objects connected with neutrinos ($l_S, \bar{l}_S$), with down quarks ($q^{'}$) and with W bosons ($U^{\pm}$, U^0). It also requires a new vector boson D, which could be as heavy as several times the Z^0 mass. The U^0 boson decays invisibly and can be produced in the reaction $e^+e^- \rightarrow U^0\bar{U^0}\gamma$, contributing to the process $e^+e^- \rightarrow \gamma$+$inv$. Also

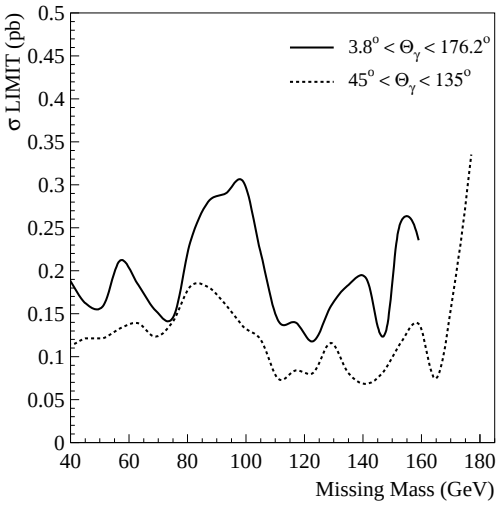

Figure 5: Limit at 95% C.L. for the production of a new unknown stable neutral object.

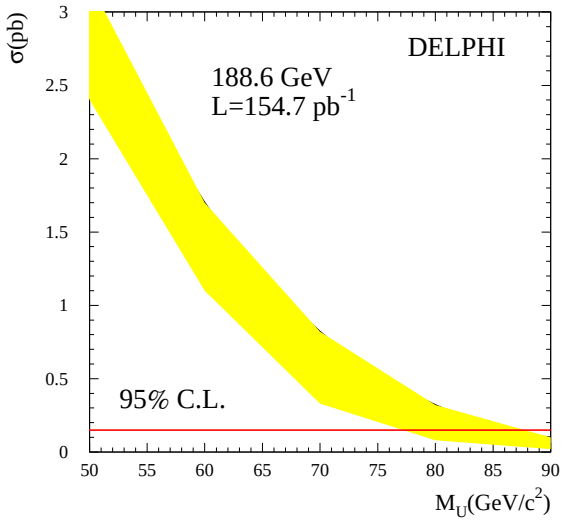

Figure 6: Limit at 95% C.L. for the mass of the W-type U boson from 189 GeV data.

pairs of $l_S\bar{l}_S$ could be produced through $U^{\pm}$ exchange and contribute to the single-photon final state.

Calculating the cross-sections with the hypothesis that a composite boson D exists with mass between $M_D = 5M_{Z^0}$ and $M_D = 7M_{Z^0}$ and adding the contributions to the cross-sections coming from direct production of $U^0\bar{U}^0$ pairs and the exchange of $U^{\pm}$, a limit can be obtained on M_U after subtracting the contribution expected from neutrino production in the Standard Model. The limit calculated from the HPC and FEMC data is shown in Figure 6 and it ranges between $M_U > 77 - 87$ GeV/c^2 at 95% C.L. when M_D is varied in the range indicated above. Weaker limits have been determined at lower LEP2 energies [2].

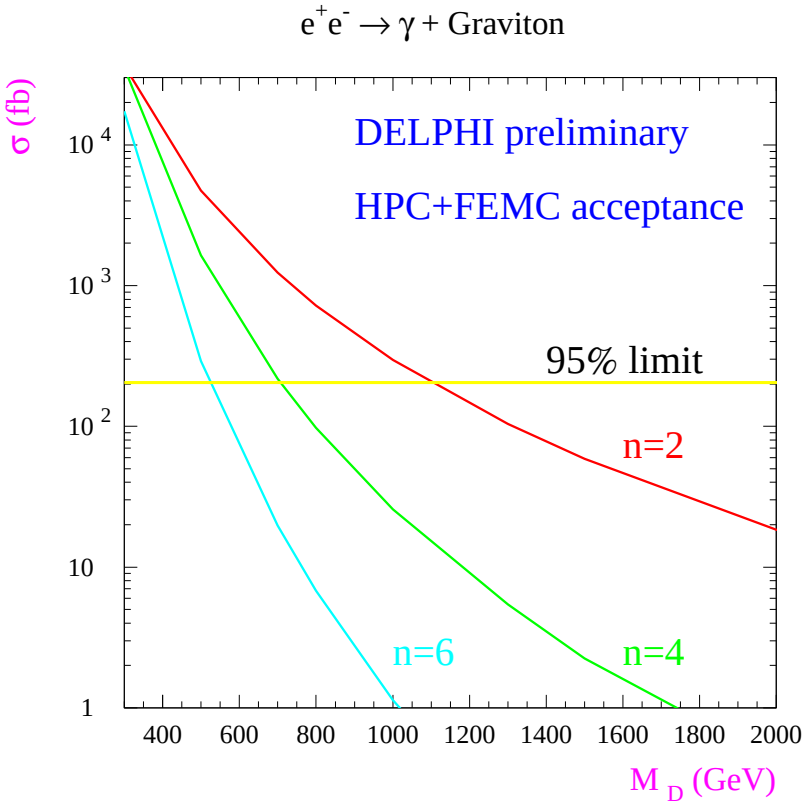

Figure 7: The cross-section limit at 95% C.L. for $e^+e^- \to \gamma G$ production and the expected cross-section for 2, 4 and 6 extra dimensions.

6.3 Limits on the production of gravitons.

It has been suggested recently [6][7][8] that gravitational interactions could be unified with gauge interactions already at the weak scale if there are extra compact dimensions of space in which only gravity can propagate. The observed weakness of gravitation compared to other forces would be related to the size of the compactified extra dimensions. A fundamental mass scale M_D is introduced, which is related to Newtons constant G_N and to the size or radius R of the compactified space (assumed to be a torus) by

$$M_D^{n+2} R^n = (8\pi G_N)^{-1}$$

where n is the number of dimensions in addition to the usual 4 dimensional space. With one extra dimension and a fundamental scale of 0.5-1 TeV, the size of this dimension becomes $10^{12} - 10^{13}$ m which is excluded by macroscopic measurements. However, already with two extra dimensions, R is in the range 0.5-1.9 mm and with n=6 the size of the dimensions becomes 0.3-0.7 Å. In this case the modification of the gravitational force would not be observable in previous gravitational measurements.

The consequence of this model is that at LEP gravity could manifest itself by the production of gravitons (G), which themselves would be undetectable by the experiments. Instead single photons from the $e^+e^- \to \gamma G$ reaction are observable. The differential cross-section for this process has been calculated [7]. Most of the signal is expected at

low photon energy (< 30 GeV) and, since $\sigma \sim s^{n/2}/M_D^{n+2}$, at the highest available center-of-mass energy. For this reason, only the HPC and FEMC data recorded at 189 GeV has been used to set a limit on the gravitational scale. The results are presented in Figure 7. A cross-section limit of

$$\sigma < 0.20 \text{ pb} \quad \text{at } 95\% \text{ C.L.} \tag{1}$$

results in limits on the fundamental mass scale of $M_D > 1.11$ TeV, $M_D > 0.70$ TeV and $M_D > 0.53$ TeV for 2, 4 and 6 extra dimensions respectively. This translates into a limit on the size of the dimensions of $R < 0.4$ mm for $n = 2$.

6.4 Limit on the mass of the gravitino

If the assumption is made that the gravitino is the lightest supersymmetric particle (LSP) and that all other supersymmetric particles are too heavy to be produced, the cross-section for the process $e^+e^- \to \tilde{G}\tilde{G}\gamma$ can be computed [4]. Lower limits on the mass of such a light gravitino has been extracted in other LEP measurements [1]. Similarly in DELPHI, the radiative double differential cross-section $d^2\sigma/(dx_\gamma, dcos\theta_\gamma)$ given in [4] for the radiative production ($e^+e^- \to \tilde{G}\tilde{G}\gamma$), was compared with the observed data.

The largest sensitivity is obtained with photons at low energy and/or low polar angle, as demonstrated in [4]. Single photon final states from the Standard Model process $e^+e^- \to \nu\bar{\nu}\gamma$ have a polar angle distribution similar to the signal, except for the enhanced characteristic peak due to the radiative return to the Z^0, at $x_\gamma = 1 - \mathrm{M_Z}^2/\mathrm{s}$. Therefore, the optimal kinematic region in which to look for the signal is in the low photon energy region. Since the signal cross-section grows as the sixth power of the center-of-mass energy, the highest sensitivity is found at the highest beam energy. For this reason, only the data taken at $\sqrt{s} = 189$ GeV has been used. The lower limit on the gravitino mass ($m_{\tilde{G}}$) can be extracted from the upper limit on the production cross-section (σ_0) through:

$$m_{\tilde{G}} > 3.8 \cdot 10^{-6} eV \left[\frac{\sqrt{s}(GeV)}{200}\right]^{3/2} \left[\frac{I}{\sigma_0}\right]^{1/4} \tag{2}$$

where I describes the kinematic region defined by the cuts.

The two DELPHI calorimeters FEMC and HPC were used in this analysis. The sensitivity was optimised for each of them, maximising the value of the function I. The different low energy regions available to the three calorimeters meant that the HPC events dominated the measurement. Combining the two calorimeters, one obtains the same limit of $\sigma_0 < 0.20$ pb at 95% C.L. as in the graviton analysis. The total kinematic region corresponds to $I = 8.4$ and the lower limit on the gravitino mass from equation (2) is

$$m_{\tilde{G}} > 8.9 \cdot 10^{-6} \text{ eV/c}^2 \quad \text{at } 95\% \text{ C.L.}$$

Since the supersymmetry-breaking scale $|F|^{\frac{1}{2}}$ is related to the gravitino mass by $|F| = \sqrt{\frac{3}{8\pi}/G_N} \cdot m_{\tilde{G}}$ the limit on the scale is $|F|^{\frac{1}{2}} > 194$ GeV. The effect of the systematic uncertainties on this limit is negligible. This limit is weaker than those obtained at $p\bar{p}$ machines [22] and by astrophysical constraints [23] and it is at the same level as those set by $(g-2)_\mu$ [24]. However, it has the feature of being valid when all the masses in the SUSY models are very large.

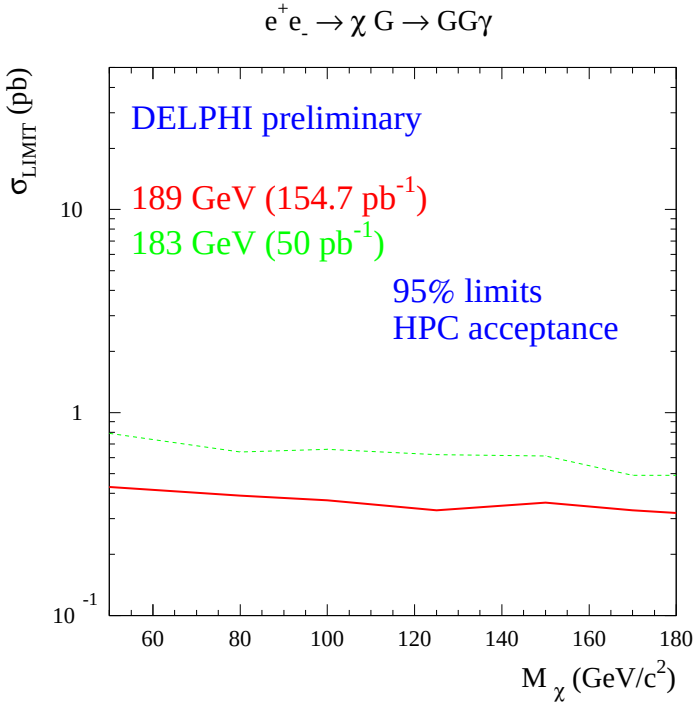

Figure 8: Upper limits for the cross-section of the process $e^+e^- \rightarrow \tilde{G}\tilde{\chi} \rightarrow \tilde{G}\tilde{G}\gamma$ at 95% C.L.

6.5 Limits on neutralino production if $\tilde{G}$ is the LSP

Supersymmetric models such as the gauge-mediated supersymmetric (GMSB) model [26] or the "no-scale" supergravity model (a.k.a. the NLZ model) [27][28] predicts that the gravitino $\tilde{G}$ is the lightest supersymmetric particle (LSP). If the next lightest supersymmetric particle (NLSP) is the neutralino $\tilde{\chi}_1^0$, both single-photon and multi-photon production can occur at LEP2 via the processes $e^+e^- \rightarrow \tilde{G}\tilde{\chi}_1^0 \rightarrow \tilde{G}\tilde{G}\gamma$ and $e^+e^- \rightarrow \tilde{\chi}_1^0\tilde{\chi}_1^0 \rightarrow \tilde{G}\gamma\tilde{G}\gamma$. While the rate of the former process is proportional to the inverse of the gravitino mass squared, the di-photon process is independent of the gravitino mass. Consequently, the single-photon process is expected to dominate only for very light gravitinos and calculations done with the NLZ model at $\sqrt{s} = 190$ GeV predicts that $e^+e^- \rightarrow \tilde{G}\tilde{\chi}_1^0 \rightarrow \tilde{G}\tilde{G}\gamma$ can be observed only if $m_{\tilde{G}} < 3 \cdot 10^{-5}$ eV [27].

The cross-section limit for $e^+e^- \rightarrow \tilde{G}\tilde{\chi}_1^0 \rightarrow \tilde{G}\tilde{G}\gamma$ was calculated from the energy distribution of the expected events, generated with *SUSYGEN* [25] and the observed single photon events in the angular region $45° < \theta < 135°$, after taking into account the expected background from $\nu\bar{\nu}\gamma$. The cut on E_γ was made in such a way as to keep at least 90% of the signal. The resulting overall efficiency, including both the energy cut and the geometrical acceptance, varied between 55% and 60% for neutralino masses ranging from 50 to 180 GeV. The calculated upper limit for the cross-section of the process $e^+e^- \rightarrow \tilde{G}\tilde{\chi}_1^0$ is given in Figure 8 for the data at 183 GeV and 189 GeV separately. A branching ratio of 100% for the process $\tilde{\chi}_1^0 \rightarrow \tilde{G}\gamma$ was assumed. The measured cross-section limit corresponds to a limit on the neutralino mass of $m_{\tilde{\chi}_1^0} > 110$ GeV if $m_{\tilde{G}} = 10^{-5}$ eV and $m_{\tilde{e}} = 150$ GeV [27].

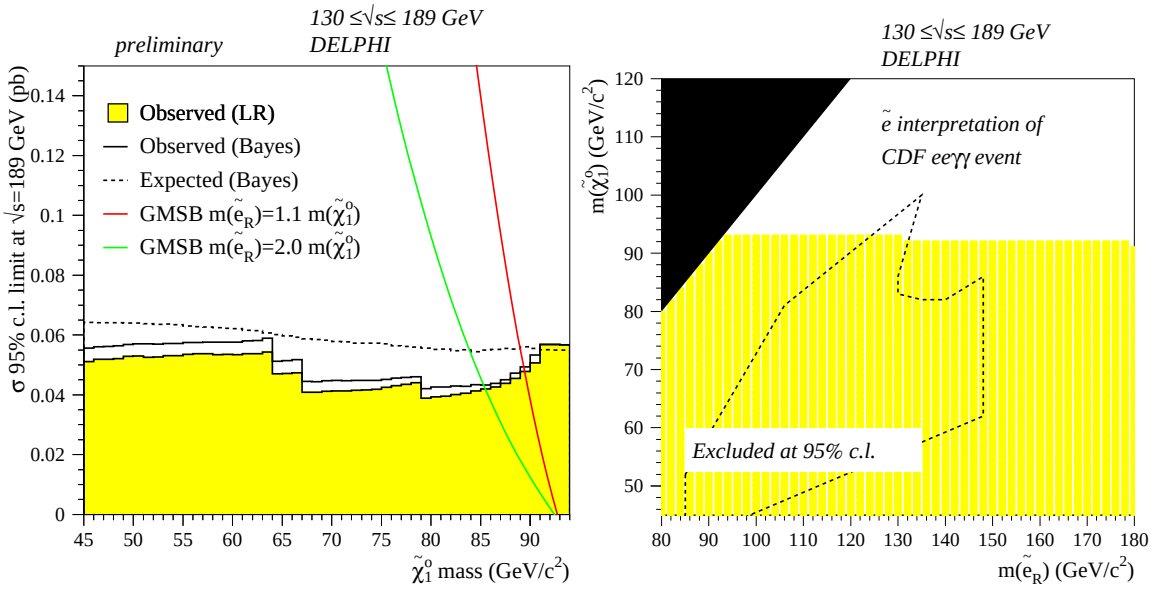

Figure 9: Left: Upper limit at 95% C.L. on the cross-section at $\sqrt{s}$ =189 GeV of the process $e^+e^- \to \tilde{\chi}_1^0\tilde{\chi}_1^0 \to \tilde{G}\gamma\tilde{G}\gamma$ as a function of the $\tilde{\chi}_1^0$ mass. The limit was obtained by combining all data taken at $\sqrt{s}$ =130-189 GeV, assuming the signal cross-section to scale as β_Y^3/s. Right: The shaded area shows the exclusion region in the $m_{\tilde{\chi}}$ versus $m_{\tilde{e}_R}$ plane, calculated from the DELPHI data at $\sqrt{s}$ =130-189 GeV. The region compatible with the selectron interpretation of the famous CDF ee$\gamma\gamma$ event [30] is also shown.

In the search for $e^+e^- \to \tilde{\chi}_1^0\tilde{\chi}_1^0 \to \tilde{G}\gamma\tilde{G}\gamma$ at $\sqrt{s}$ =189 GeV, 5 events were observed with 4.4 expected from $e^+e^- \to \nu\overline{\nu}\gamma\gamma(\gamma)$, which is the dominant standard model background. This bring the total number of events found at $\sqrt{s}$ =130-189 GeV to 7 with 7.1 expected (Table 4). Figure 9 shows the cross-section limit calculated from these events as a function of the $\tilde{\chi}_1^0$ mass (assuming a branching ratio of 100% for $\tilde{\chi}_1^0 \to \tilde{G}\gamma$) and the exclusion region in the $m_{\tilde{\chi}}$ versus $m_{\tilde{e}_R}$ plane. The expected cross-section for $e^+e^- \to \tilde{\chi}_1^0\tilde{\chi}_1^0 \to \tilde{G}\gamma\tilde{G}\gamma$ in Figure 9 has been calculated with the GMSB model for two different assumptions about the selectron mass.

If the gravitino mass is larger than 200-300 eV, the $\tilde{\chi}_1^0$ can have such a long lifetime that it will decay in the detector. The signature for this case is photons that do not point to the interaction region. If the decay length is long, the probability to detect both photons is small and therefore single photon events were searched for which had a shower axis reconstructed in the HPC which gave a beam crossing point at least 40 cm away from the interaction point [10]. Four events were found at 189 GeV with 5.2 expected bringing the total at all energies to 6 and 7.9 (Table 4).

Figure 10 shows the cross-section limit as a function of the mean decay path of the neutralino using both the multi-photon events and the non-pointing single photon events.

6.6 Limits on neutralino production if $\tilde{\chi}_1^0$ is the LSP

In other SUSY models [29] the $\tilde{\chi}_1^0$ is the LSP and $\tilde{\chi}_2^0$ is the NLSP. The single-photon production in this scenario via $e^+e^- \to \tilde{\chi}_2^0\tilde{\chi}_1^0 \to \tilde{\chi}_1^0\tilde{\chi}_1^0\gamma$ has a lower cross-section times

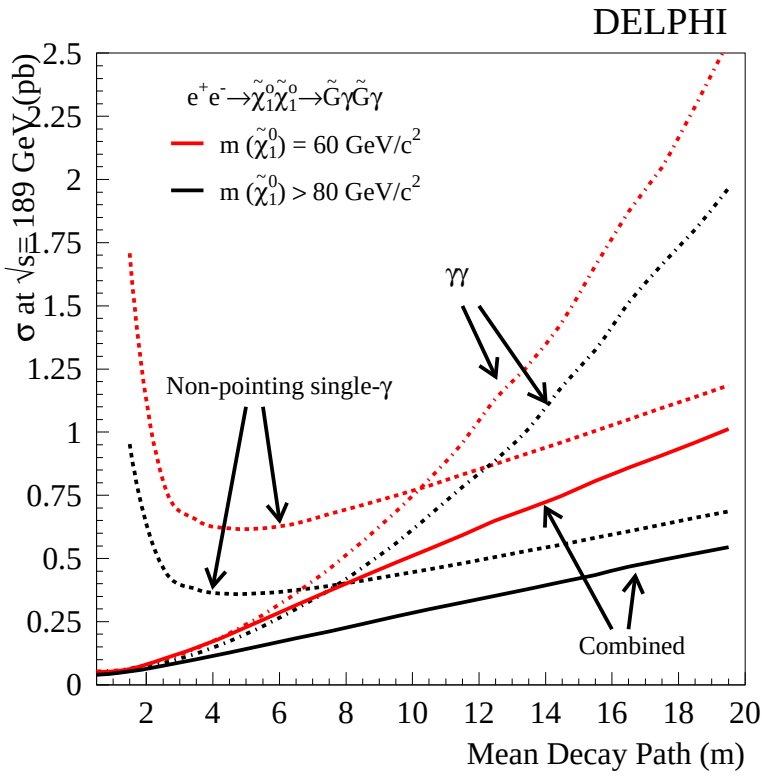

Figure 10: Upper limit at 95% C.L. on the cross-section at $\sqrt{s}$ =189 GeV of the process $e^+e^- \to \tilde{\chi}_1^0\tilde{\chi}_1^0 \to \tilde{G}\gamma\tilde{G}\gamma$ as a function of the $\tilde{\chi}_1^0$ mean decay path for two hypotheses on the neutralino mass: $m_{\tilde{\chi}} = 60$ GeV and 80 GeV$< m_{\tilde{\chi}} < \sqrt{s}$.

branching ratio than $e^+e^- \to \tilde{\chi}_2^0\tilde{\chi}_2^0 \to \tilde{\chi}_1^0\gamma\tilde{\chi}_1^0\gamma$ except when the masses of $\tilde{\chi}_1^0$ and $\tilde{\chi}_2^0$ are very close.

The $e^+e^- \to \tilde{\chi}_2^0\tilde{\chi}_2^0 \to \tilde{\chi}_1^0\gamma\tilde{\chi}_1^0\gamma$ process has an experimental signature which is the same as for $e^+e^- \to \tilde{\chi}_1^0\tilde{\chi}_1^0 \to \tilde{G}\gamma\tilde{G}\gamma$ but with somewhat different kinematics due to the masses of the $\tilde{\chi}_1^0$. The previous DELPHI analysis at lower energies [10] has now been repeated with the 189 GeV data sample. Eight events remains after all cuts with 5.2 expected from the standard model background (Table 4). Figure 11 shows the cross-section limit calculated from the events collected at all energies as a function of the $\tilde{\chi}_1^0$ and $\tilde{\chi}_2^0$ masses, assuming a branching ratio of 100% for $\tilde{\chi}_2^0 \to \tilde{\chi}_1^0\gamma$.

7 Conclusions

With the 209 pb^{-1} of data collected by DELPHI in 1997 and 1998 at a center-of-mass energy of 183 GeV and 189 GeV, a study has been made of the production of events with a single photon in the final state and no other visible particles. Previous results on single non-pointing photons and on multi-photon final states have also been updated with 189 GeV data.

The measured single-photon cross-sections are in agreement with the expectations from the Standard Model process $e^+e^- \to \nu\bar{\nu}\gamma$ and the number of light neutrino families is measured to be:

$$N_\nu = 2.88 \pm 0.13(stat) \pm 0.14(syst)$$

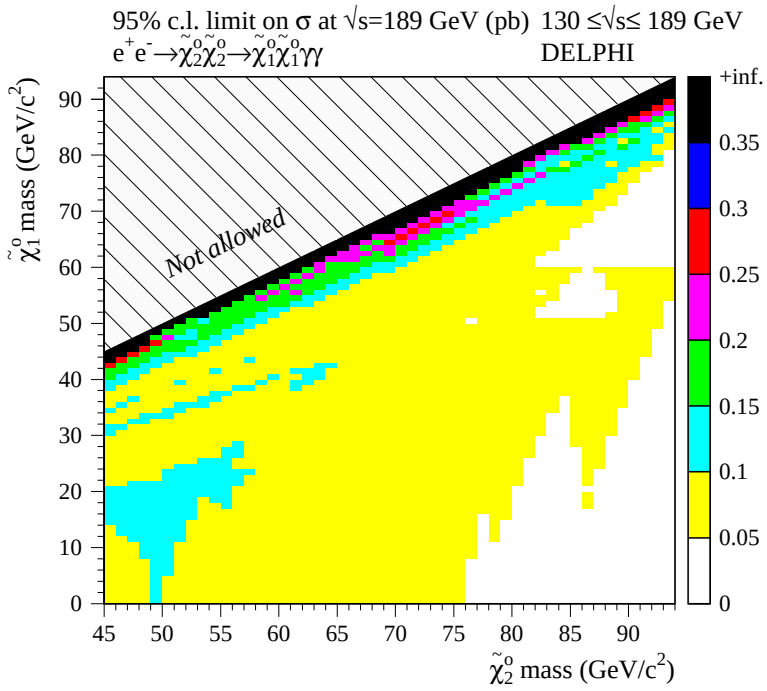

Figure 11: Upper limit at 95% C.L. on the cross-section at $\sqrt{s}$ =189 GeV of the process $e^+e^- \to \tilde{\chi}_2^0\tilde{\chi}_2^0 \to \tilde{\chi}_1^0\gamma\tilde{\chi}_1^0\gamma$ as a function of the $\tilde{\chi}_1^0$ and the $\tilde{\chi}_2^0$ mass. The limit was obtained by combining all data taken at $\sqrt{s}$ =130-189 GeV, assuming the signal cross-section to scale as β_Y^3/s.

The absence of an excess of events with one or more photons in the final state has been used to set limits on the production of a new unknown model-independent neutral state, a W-type U-boson as described by a composite model, gravitons propagating in high-dimensional space, a light gravitino and neutralinos.

References

[1] ALEPH Collaboration, R. Barate *et al.*, Phys. Lett. **B420** (1998) 127.
ALEPH Collaboration, R. Barate *et al.*, Phys. Lett. **B429** (1998) 201.
L3 Collaboration, M. Acciarri *et al.*, Phys. Lett. **B411** (1997) 373;
L3 Collaboration, M. Acciarri *et al.*, Phys. Lett. **B444** (1998) 503;
OPAL Collaboration, K. Ackerstaff *et al.*, Eur. Phys. J. C2(1998) 607;
OPAL Collaboration, K. Ackerstaff *et al.*, Eur. Phys. J. C8(1999) 23.

[2] DELPHI Collaboration, P. Abreu *et al.*, Phys. Lett. **B380** (1996) 471.

[3] DELPHI Collaboration, P. Ferrari *et al.*, DELPHI NOTE 98-76 CONF 144, contrib. to the ICHEP'98 conference in Vancouver, Canada, July, 1998.

[4] A. Brignole, F. Feruglio and F. Zwirner, Nucl. Phys. **B516** (1998) 13.

[5] H. Senju, Prog. Theor. Phys. **95** (1996) 455 and references therein.

[6] N. Arkani-Hamed, S. Dimopoulos and G. Dvali, Phys. Lett. **B429** (1998) 263.

[7] G.F. Giudice, R. Rattazzi and J.D. Wells, Nucl. Phys. **B544** (1999) 3.

[8] E.A. Mirabelli, M. Perelstein and M.E. Peskin, Phys. Rev. Lett. **82** (1999) 2236.

[9] S. Ambrosanio and B. Mele, Phys. Rev. **D52** (1995) 3900;
S. Ambrosanio *et al.*, Nucl. Phys. **B478** (1996) 46.

[10] DELPHI Collaboration, P. Abreu *et al.*, Eur. Phys. J. C6(1999) 37.

[11] DELPHI Collaboration, P. Abreu *et al.*, Nucl. Inst. and Meth. **A378** (1996) 57;
DELPHI Collaboration, P. Aarnio *et al.*, Nucl. Inst. and Meth. **A303** (1991) 233.

[12] S.J. Alvsvaag *et al.*, Nucl. Inst. and Meth. **A425** (1999) 106.

[13] DELPHI Collaboration, DELPHI 89-67 PROG 142;
DELPHI Collaboration, DELPHI 89-68 PROG 143.

[14] D. Karlen, Nucl. Phys. **B289** (1987) 23.

[15] M. Caffo, R. Gatto and E. Remiddi, Phys. Lett. **B173** (1986) 91;
M. Caffo, R. Gatto and E. Remiddi, Nucl. Phys. **B286** (1987) 293.

[16] E. Falk, V. Hedberg and G. von Holtey, CERN SL/97-04(EA).

[17] S. Jadach *et al.*, Comp. Phys. Comm. **66** (1991) 276;
S. Jadach *et al.*, Comp. Phys. Comm. **79** (1994) 503.

[18] G. Montagna *et al.*, Nucl. Phys. **B452** (1995) 161.

[19] DELPHI Collaboration, P. Abreu *et al.*, Eur. Phys. J. C1(1998) 1.

[20] DELPHI Collaboration, P. Abreu *et al.*, Z. Phys. **C74** (1997) 577.

[21] OPAL Collaboration, R. Akers *et al.*, Z. Phys. **C65** (1995) 47.

[22] D. Dicus and S. Nandi, Phys. Rev. **D56** (1997) 4166;
A. Brignole *et al.*, Nucl. Phys. **B526** (1998) 136.

[23] J.A. Grifols, Pramana **51** (1998) 135.

[24] F. Ferrer and J.A. Grifols, Phys. Rev. **D56** (1997) 7466;
T. Li, J.L. Lopez and D.V. Nanopoulos, Preprint hep-ph/9704439.

[25] S. Katsanevas and P. Morawitz, Comp. Phys. Comm. **112** (1998) 227.

[26] S. Dimopoulos *et al.*, Phys. Rev. Lett. **76** (1996) 3494.

[27] J. L. Lopez *et al.*, Phys. Rev. Lett. **77** (1996) 5168.

[28] J. L. Lopez *et al.*, Phys. Rev. **D55** (1997) 5813.

[29] S. Ambrosiano *et al.*, Phys. Rev. **D55** (1997) 1392.

[30] The CDF collaboration, F. Abe *et al.*, Phys. Rev. Lett. **81** (1998) 1791.